ISSN 1070-3284, Russian Journal of Coordination Chemistry, 2015, Vol. 41, No. 11, pp. 751–758. © Pleiades Publishing, Ltd., 2015.

Coordination Compounds as the Precursors for Preparation of Nanosized Platinum or Platinum-Containing Mixed-Metal Catalysts of Oxygen Reduction Reaction[1]

V. A. Grinberg[a, *], V. V. Emets[a], N. A. Mayorova[a], A. A. Pasynskii[b], A. A. Shiryaev[a], V. V. Vysotskii[a], V. K. Gerasimov[a], V. V. Matveev[a], E. A. Nizhnikovskiy[a], and V. N. Andreev[a]

[a] *Frumkin Institute of Physical Chemistry and Electrochemistry, Russian Academy of Sciences, Moscow*

[b] *Kurnakov Institute of General and Inorganic Chemistry, Russian Academy of Sciences, Moscow*

**e-mail: vgrinberg@phyche.ac.ru*

Received February 26, 2015

Abstract—Nanosized mixed-metal platinum–iron, platinum–manganese and platinum–nickel catalysts supported on highly dispersed carbon black are synthesized by using the corresponding metal complexes with the atomic metal ratio of 1 :1 . The obtained catalysts are characterized by X-ray phase diffraction and scattering analysis, electron dispersion analysis, scanning and transmission electron microscopy. Thin film rotating disk electrode technique was used to study kinetic parameters of the oxygen reduction reaction at these catalysts. It has been demonstrated that electrochemical activity of the prepared catalysts is comparable to that of a commercial E-Tek platinum catalyst. The membrane electrode assembly (MEA) with the synthesized platinum-iron catalyst was tested in a laboratory hydrogen-air fuel cell setup at room temperature. It was shown that the power performance of this MEA was twice better than that of a MEA on the base of a commercial Pt/C E-Tek catalyst.

DOI: 10.1134/S1070328415110020

INTRODUCTION

Hydrogen-oxygen fuel cells (FCs) belong to most promising self-contained electric power sources, particularly for electromobiles, some stationary and portable devices. Among diverse FC types the most suitable devices for these purposes are low temperature hydrogen-oxygen (air) FCs with ion-exchange membranes fueled by pure hydrogen or hydrogen obtained by conversion of liquid organic fuels. Such devices are characterized by high performance, enhanced power density (W cm^{-2}), sufficient lifetime; they are environmentally friendly and compact. So far, the technology of production of such elements is generally developed, but serious problems hampering large-scale FC application still exist. The most important problems include not only hydrogen production, purification, and storage, but also development of more efficient electrocatalysts that would provide longer FC operation without deterioration of their characteristics, would contain minimum amounts of noble metals, would be inexpensive and processable.

It is well known that characteristics of hydrogen-oxygen FCs depend mainly on the rate of the cathodic oxygen reduction reaction. To enhance the efficiency of catalysts in this reaction, multicomponent, particularly binary, Pt-based metallic nanosized systems (Pt–Co, Pt–Ni, Pt–Cr, Pt–Fe, etc.), that are also tolerant towards organic admixtures, are studied extensively [1–10]. However the results obtained are often controversial. Thus, in some works the authors observed true catalytic effects after introduction of the second metal, i.e., an increase in kinetic current per true surface area or per single surface platinum atom [7]. In other cases an increase in current was related to a partial etching of the basic metal component and therefore to an increase in the alloy true surface area [1]. In some cases an advantage of binary catalysts was manifested largely in their tolerance towards methanol [10]. Different mechanisms of the catalytic effect are also discussed: a change in the length of the Pt–Pt interatomic bond as a result of alloy formation [5], inhibition of the water decomposition reaction due to formation of the surface Pt–OH groups hindering oxygen adsorption [8], the Fermi level effect [10, 11] or combined influence of structural factors and variation in the electronic state of metals in the alloy [6, 12]. It should be noted that the phase composition and structure of binary systems are varied from mixed deposits (Pt–Cr [10]) to solid solutions (Pt–Co, Pt–Ni [7]) and intermetallides with the composition Pt_3Me (Pt_3Co, Pt_3Fe [8]). Analysis of literature data shows that the observed catalytic effects and their mechanism are determined not only by the chemical nature of a binary catalyst, but also by its structure and phase composition that, in turn, depend on the method of synthesis.

[1] The article is published in the original.

In the case of co-reduction of the salts of different metals, one often fails to obtain a catalyst of a given composition and structure due to difference in the rates of metallization processes. In this work binary catalysts were synthesized from precursors of coordination complexes of platinum and other metals. Impregnation of a suitable support by a solution of such compounds and removal of organic shell of the metal core by thermodestruction allows obtaining a homogeneous heterometallic coating on the support surface [13]. Herewith, the ratio of Pt : Me in the metal core of the precursor can be varied in a sufficiently wide range. The processes of thermal decomposition can be controlled using differential thermal analysis, thermogravimetry, and differential scanning calorimetry.

This work reports results of investigation of binary catalysts of the oxygen reduction reaction, namely: PtFe/C, PtMn/C, and PtNi/C. For comparison, measurements were also carried out on samples of a catalyst obtained with clustered Pt only (specifically, from ethoxy-dicyclopentadienyl-platinum-ethoxide $(C_{10}H_{12}OC_2H_5)_2Pt_3(OC_2H_5)_4$), and on a commercial E-Tek platinum catalyst (20 wt % Pt on Vulcan XC-72).

EXPERIMENTAL

Preparation of binary catalysts. Ethoxy dicyclopentadiene–platinum–ethoxide $(C_{10}H_{12}OC_2H_5)_2Pt_3(OC_2H_5)_4$ was chosen as the initial platinum compound for synthesis of heteroorganometallic precursors. Commercial coordination complexes of iron, manganese, and nickel were used as its partners, namely: $[CpFe(CO)_2]_2$, $HOOCC_5H_4Mn(CO)_3$, $(\alpha\text{-Pic})_2Ni(OOCCMe_3)_2$. For the synthesis a multistep procedure was used: (1) sonication of highly dispersed Ketjen Black (the specific surface area 600 m^2g^{-1}) in absolute tetrahydrofuran (THF); (2) dropwise addition of the corresponding mixed precursors solution in THF; (3) sonication, (4) drying at 100°C under vacuum; (5) annealing at 500°C in a hydrogen atmosphere for 45 min; (6) cooling in the atmosphere of a high-purity argon. The obtained catalysts contained 30 wt % of the metals and 70 wt % of the carbon black. The atomic ratio of the metals in binary systems was close to 1 : 1.

Structural studies. Studies of morphology and structure in the initial state and after electrochemical polarization were carried out using a Quanta 650 FEG scanning electron microscope (SEM) equipped with a field emission cathode (FEI, Netherlands) and an energy-dispersive detector.

X-ray phase analysis was carried out using an Empyrean diffractometer (Panalytical) with filtered CuK_α radiation in the standard Bragg–Brentano geometry ("reflection"). Samples were studied in the absence of binders.

Small-angle X-ray scattering measurements were performed using a specialized SAXSess diffractometer (Anton Paar). Samples in an envelope of non-scattering polymer were analyzed at room temperature in the transmission geometry; the sample chamber was evacuated; imaging plates were used as detectors. Experimental curves were normalized for sample absorption; standard desmearing procedures were applied. Particle size distribution was calculated after subtraction of initial carbon support scattering according to the Tikhonov regularization method using a GNOM software [14]. The average particle size and size distribution were also determined using a Philips EM-301 transmission electron microscope at the accelerating voltage 80 kV.

Electrochemical measurements. Electrochemical studies were carried out using PI-50.1 or PAR 273A potentiostats. Measurements on a rotating disk electrode were carried out using an EL-02.06 potentiostat. The true surface area of supported metallic catalysts was determined by anodic stripping of the carbon monoxide monolayer [15].

Thin film rotating disk electrode (TFRDE) technique was used to estimate kinetic currents of the oxygen reduction at the studied catalysts [7–10, 15]. The electrochemical cell and TFRDE manufacturing procedure are described in detail in [16]. The aqueous catalyst suspension stabilized by sonication was transferred to the surface of a glassy carbon disk electrode (the surface area 0.07 cm^2) in the amount 21 μg cm^{-2} (per platinum). After drying in air at 60°C the catalyst layer was fixed on the electrode surface using a Nafion (Aldrich) 0.05% aqueous solution. The calculated thickness of the Nafion film after drying was 0.15 μm. All TFRDE measurements were performed in a 0.5 M H_2SO_4 solution prepared from extra-pure grade sulfuric acid and deionized water; the solution was oxygen saturated under atmospheric pressure. A platinum gauze (~10 cm^2) served as the counter electrode and a Hg/Hg_2SO_4/0.5 M H_2SO_4 was used as the reference electrode. Compressed gases were used to argon purge the solution or to saturate it with oxygen. All measurements were performed at room temperature.

Thin film RDE was cleaned and activated electrochemically by cycling its potential in the range 0.0–1.2 V in case of monoplatinum and in the range 0.0–1.0 V in case of bimetallic catalysts.

The study of the ORR kinetics was carried out by cyclic voltammetry over the potential range 1.1–0.2 V at a scan rate of 5 mV s^{-1} and the electrode rotation speed ~2000 rpm. Reproducibility of the current measurements was ±5–6%. In order to estimate stability of the synthesized catalysts under working conditions, accelerated tests in a continuous electrode cycling mode were carried out in the potential range 0.2–1.0 V at a scan rate of 100 mV s^{-1} under continuous bubbling of the solution by oxygen (500 cycles followed by analysis of the catalytic layer composition). The experimental data obtained were processed using the standard software.

The activity of the studied catalysts in the reaction of molecular oxygen reduction was analyzed in this work at the electrode potential values 0.8–0.9 V (here and after the potentials are given vs. the hydrogen electrode in the same solution), which are close to a currentless potential of the cathode in a hydrogen–oxygen fuel cell. Comparison of the kinetic currents obtained at different catalysts allowed estimating the activity of the latter along with a degree of their purification from precursors and other impurities.

RESULTS AND DISCUSSION

Analysis of phase composition of the synthesized bimetallic catalysts was performed by X-ray diffraction analysis using the JCPDS–ICDD database. Diffractograms of the initial carbon support and of the Pt/C, PtMn/C, PtFe/C, and PtNi/C samples are shown in Fig. 1. Though line broadening due to nanodimensions of the studied phases hindered unambiguous identification of metal-containing particles, the presence of metallic particles and phases with composition Pt_3Fe, PtFe, $PtMn_3$, PtMn, Pt_3Ni, and some other Pt–Ni compounds is plausible. Besides, an admixture of well crystallized manganese oxides and of the $Pt_{0.63}Mn_{0.37}$ phase was observed in the PtMn/C sample.

The crystallite size (according to the Debye–Scherrer formula) in the PtFe/C sample was in the range 1.7–4.7 nm (dependent on reflection), in the PtMn/C sample—2.3–6.6 nm, and in the PtNi/C sample—8–19 nm. Unfortunately, the ambiguity of phase determination and superposition of peaks obviously impairs the accuracy of the obtained values, which is indirectly confirmed by analysis of the electron microscopy and small angle X-ray scattering data. As will be shown further, considerable discrepancy between the XRD-derived crystallite sizes for the PtNi/C sample and the SAXS and TEM data is possibly related to the fact that small particles are poorly crystalline and the Debye–Scherrer formula emphasizes the contribution of "high-quality" large particles.

Small-angle scattering curves after subtracting the contribution of the carbon support for the PtFe/C and PtMn/C samples are shown in Fig. 2. Particle size distribution was calculated at the assumption of their spherical shape; the distribution was forced to pass through origin (Fig. 3). The calculated size distribution is rather robust, but is only weakly dependent on the maximum scatterer size.

The Guinier plot ($\log(I) - q^2$) contains extensive linear regions pointing to the existence of monodispersed particles with the gyration radii of 1.17 nm for Pt–Fe, 1.2 nm for Pt–Ni, and 1.38 nm for Pt–Mn. The obtained values are close to the sizes of the coherent scattering regions calculated on the basis of diffraction data and to the maximum in the particle size distribution curve. Note that the slope of the scattering curves in the log-log scale is close to –2. In case of

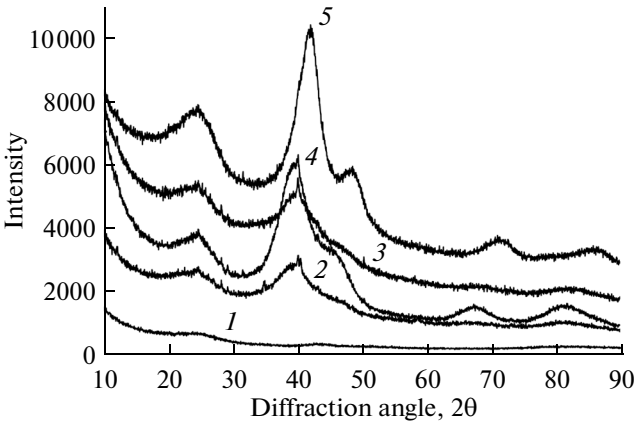

Fig. 1. X-ray diffraction patterns: carbon support (*1*); PtMn/C (*2*); PtFe/C (*3*); Pt (*4*); PtNi/C (*5*).

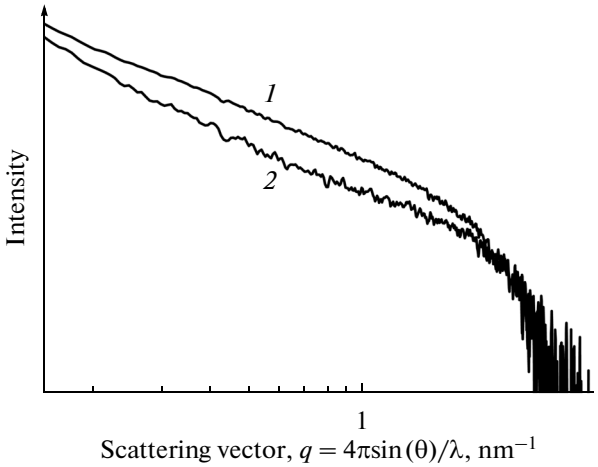

Fig. 2. Small-angle X-ray scattering: PtFe/C (*1*); PtMn/C (*2*).

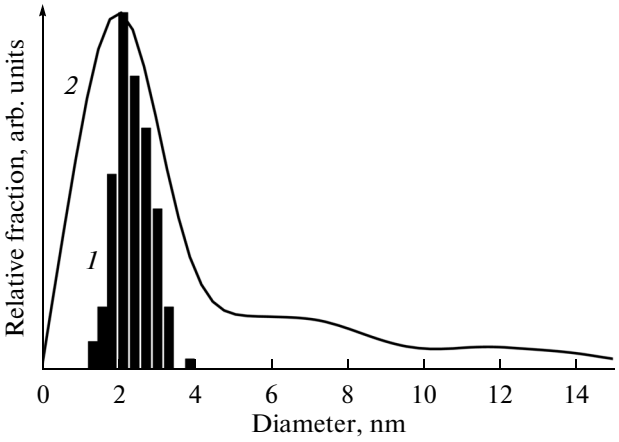

Fig. 3. Comparison of particles size distribution extracted from TEM (histogram) and from SAXS (solid curve) data for PtMn/C sample: TEM (*1*); SAXS (*2*).

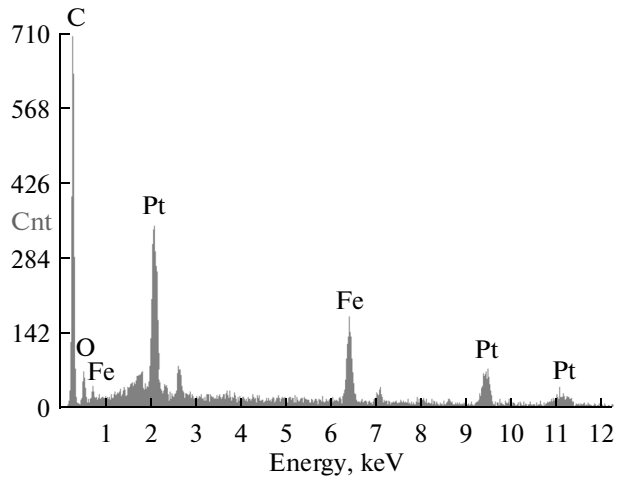

Fig. 4. EDX spectrum of the synthesized platinum–iron catalyst sample.

small polydispersity, such behavior of the curve points to a disk-like shape of the scatterers.

Figure 3 compares the distribution of particle sizes in the PtMn/C sample obtained from the small-angle scattering and TEM data.

Figure 4 shows a typical EDX spectrum of the PtFe/C sample; the chemical composition of the PtFe/C, PtMn/C, and PtNi/C samples is given in Table 1.

It should be noted that the ratio of metallic components of the synthesized PtFe/C, PtMn/C, and PtNi/C catalyst samples is within the following limits: Pt : Fe = 1 : (1.11–1.18), Pt : Mn = 1 : (1.07–1.25), Pt : Ni = 1 : 1.25. Thus, a small excess of the non-platinum component is observed. A similar phenomenon of the surface layer enrichment by less noble component was also observed earlier for alloys dispersed on carbon black [13].

As seen in Figs. 5b–5e, the average particle size of the monoplatinum and the binary PtFe/C and PtMn/C catalysts is between 2 and 2.5–3.0 nm; besides, a small amount of particles with an average size of 3 to 7 nm is also present in the samples. At the same time, the average particle size in the PtNi/C catalyst is 7 nm and the sample contains particles with the size up to 25 nm.

Surface morphology of the PtFe/C, PtMn/C, and PtNi/C catalysts studied using the SEM method before and after prolonged cycling in the oxygen-saturated electrolyte remains practically unchanged. At the same time, according to EDX spectra, the surface composition changes considerably: iron and manganese are virtually absent in the surface layer of respective samples after the cycling (Table 2) probably due to their dissolution in the course of electrochemical process (as discussed below). One should note that a similar phenomenon was observed by other researchers. Thus, in [1], the cycling of the $Pt_{0.8}Cr_{0.2}$ alloy electrode resulted in enrichment of the surface by platinum due to dissolution of the less noble chromium, while in [7], a small decrease in the amount of surface platinum atoms as compared to the bulk composition was observed for the PtCo/C and PtNi/C alloys of different composition dispersed on carbon black.

The value of specific electrochemically active surface area of the synthesized catalysts was determined from the amount of electricity consumed at the oxidation of a pre-adsorbed carbon monoxide monolayer (in the assumption that the limiting coverage by adsorbed CO particles is 100%). The specific surface area values were 187, 188, 217, and 192 $m^2 g^{-1}$ for the Pt/C, PtFe/C, PtMn/C, and PtNi/C samples, respectively. Thus, the dispersity of the synthesized catalysts was comparable to that of platinum in a commercial E-Tek catalyst (its specific surface area value measured at the thin film electrode manufactured in a similar way from the commercial Pt/C E-Tek catalyst was 213 $m^2 g^{-1}$). High dispersity of the catalysts obtained on the basis of complex compounds of the corresponding metals with the atomic metal ratio 1 : 1 and of the cluster-based monoplatinum catalyst is in agreement with the values of particle size calculated from TEM and SAXS measurements.

Figure 6 shows typical voltammograms recorded at the studied catalyst electrodes (platinum loading in all cases was 21 μg cm^{-2}) in the Ar purged 0.5 M sulfuric acid solution. As shown in Fig. 6, both in case of the mono-platinum catalyst (curve *I*) and in case of bime-

Table 1. Composition of the synthesized catalysts

Catalyst	Metal	Weight composition, wt %	Atomic composition, at %
PtFe/C	Pt	17.15	1.43
	Fe	5.76	1.68
PtMn/C	Pt	19.17	1.69
	Mn	5.77	1.81
PtNi/C	Pt	20.50	1.74
	Ni	7.63	2.15

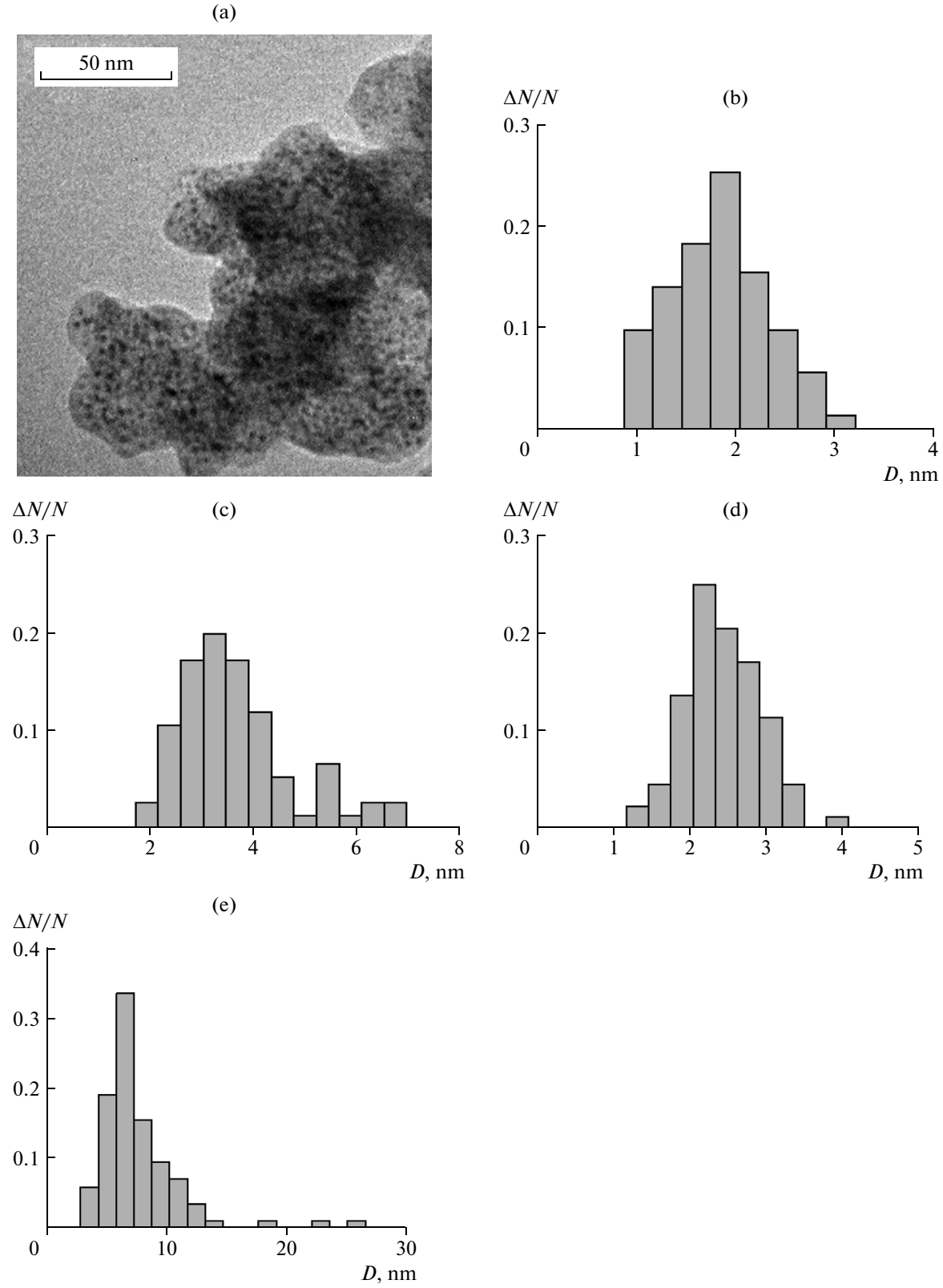

Fig. 5. Microphotograph of Pt/C sample (a) and histograms of particle size distribution (b–e) for (b) Pt/C, (c) PtFe/C, (d) PtMn/C, and (e) PtNi/C.

Table 2. Surface composition of the synthesized catalysts before and after electrochemical tests in oxygen saturated 0.5 M H_2SO_4 (500 cycles in the potential range 0.2–1.0 V)

Catalyst sample	Content of components, at %	
	initial	after polarization
PtFe/C	Pt 1.43; Fe 1.68	Pt 1.0; Fe: not found
PtMn/C	Pt 1.69; Mn 1.81	Pt 1.24; Mn 0.08
PtNi/C	Pt 1.74; Ni 2.15	Pt 1.35; Ni 0.28

tallic catalysts (curves *2–4*), voltammograms in the potential range 0.0–0.4 V are typical for supported platinum catalysts, which points to a sufficiently high degree of purification of the synthesized catalysts from precursors or other impurities. At the same time, the bimetallic catalysts are characterized by larger currents (as compared to the mono-platinum catalyst) in the double layer potential region (0.4–0.6 V). Apparently, in the case of binary catalysts some additional redox processes related to the presence of the second metal may occur at the catalyst surface. Although the decrease in the second metal content during the express stability tests (Table 2) points to the oxidation of non-noble metal components of the catalysts (Fe, Mn, Ni) in the course of prolonged electrode polarization, one must point out that the catalysts' activity in the oxygen reduction reaction remains practically unchanged.

Figure 7a shows voltammograms of the oxygen reduction at the synthesized catalysts in the range 0.2–1.1 V recorded at the potential scan rate 5 mV s^{-1} and the electrode rotation speed 2000 rpm in a 0.5 M sulfuric acid oxygen-saturated solution. The dependences for all synthesized catalysts are typical for Pt-containing catalysts; herewith, the onset potential of the oxygen reduction reaction grows (becomes more positive) in the series: Pt/C < PtNi/C ≈ PtMn/C < PtFe/C.

As a result, the values of current densities of the oxygen reduction in the potential range characteristic for an operating fuel cell cathode (0.85–0.90 V) at the bimetallic catalysts studied are 1.5–2 times higher than

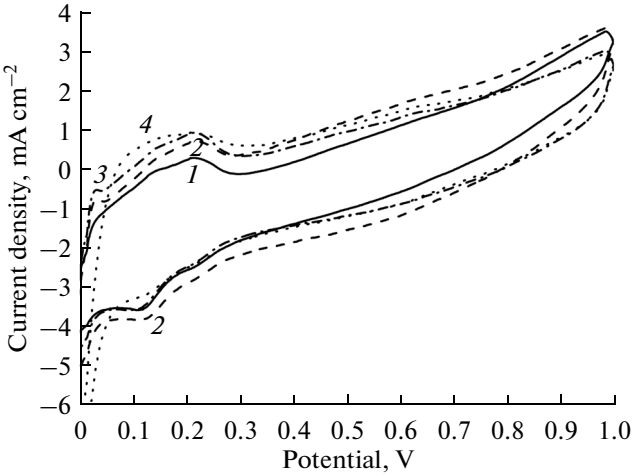

Fig. 6. Cyclic voltammograms measured at Pt/C (*1*), PtFe/C (*2*), PtMn/C (*3*), and PtNi/C (*4*) in 0.5 M H_2SO_4 solution at the potential sweep rate 20 mV s^{-1}. Platinum loading for all electrodes is 21 μg cm^{-2}.

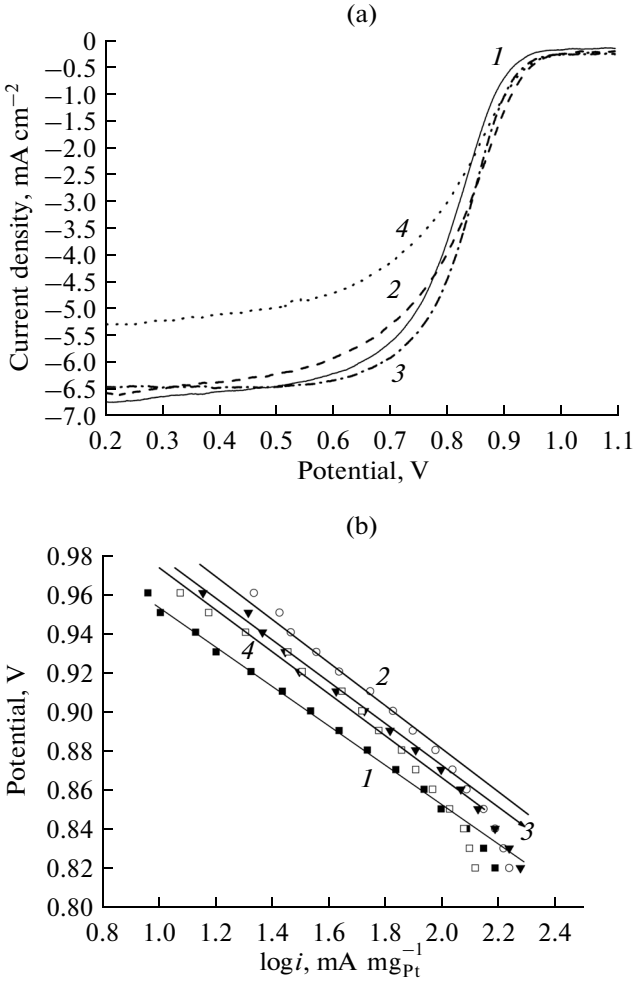

Fig. 7. Voltammograms (a) and Tafel plots (b) of the oxygen reduction at Pt/C (*1*), PtFe/C (*2*), PtMn/C (*3*), and PtNi/C (*4*) in 0.5 M H_2SO_4 solution saturated by oxygen at the atmospheric pressure measured at the potential sweep rate 5 mV s^{-1} and the electrode rotation rate 2000 rpm. Platinum loading for all electrodes is 21 μg cm^{-2}.

Table 3. Kinetic parameters of the oxygen electroreduction at Pt/C, PtFe/C, PtMn/C, and PtNi/C samples in 0.5 M H_2SO_4 (the solution is saturated by oxygen at the atmospheric pressure)

Catalyst sample	Platinum loading, μg cm^{-2}	Current density at 0.9 V, mA cm^{-2}	Specific current density at 0.9 V, mA mg_{Pt}^{-1}	True current density at 0.9 V, mA cm_{true}^{-2}	References
Pt/C	21	0.75	35.7	0.019	This work
PtFe/C	21	1.40	66.7	0.035	This work
PtMn/C	21	1.15	54.8	0.025	This work
PtNi/C	21	1.10	52.4	0.028	This work
Pt/Vulcan (E-Tek)	14	0.32	23.0	0.035	[18]

those at the monoplatinum catalyst. One can assume that the presence of Ni, Mn, and especially Fe in the platinum catalyst causes a positive catalytic effect. Similar results for binary alloys were observed in [17].

This effect is also illustrated by Fig. 7b, in which the same voltammetric dependences are presented in semi-logarithmic coordinates. As one can see, the slopes of the linear regions are close for all studied catalyst samples and correspond to 120–140 mV, which is characteristic for platinum catalysts supported on carbon. One should point out that the length of a linear section decreases somewhat when the second metal is introduced this phenomenon being most pronounced for the PtNi/C catalyst. This may point to an appearance of some additional diffusion limitations related to the presence and electrochemical conversions of the second metal and to a decrease in the relative content of the basic catalytic component, platinum, at the catalyst surface.

Table 3 shows kinetic parameters of the oxygen electroreduction at the synthesized catalysts.

The synthesized PtFe/C catalyst sample was used as a cathode material in a membrane electrode assembly tested in a laboratory hydrogen-air fuel cell setup. The membrane electrode assembly (MEA) was formed using a Nafion 212 membrane; the synthesized PtFe/C sample and a commercial E-Tek 40% Pt/C were used as the cathode and the anode catalyst, correspondingly. "Catalytic ink" for the active layer formation was prepared by ultrasonic homogenization of a catalyst sample and an ionomer solution in a water–alcohol mixture. The obtained suspension was sputtered onto a gas-diffusion layer (GDL) by using of aerograph. Sigracet 35CC was used as both the cathode and the anode GDL. The GDL surface area was 5 cm^2, while the active layer area was 1 cm^2. Platinum loading at the cathode was 0.32 mg_{Pt} cm^{-2}, and that at the anode was 0.34 mg_{Pt} cm^{-2}. For comparison, another MEA was assembled by the same procedure, but with the commercial platinum catalyst used for both the cathode and anode.

Both MEAs were tested in an ElectroChem test fuel cell with the working surface area 5 cm^2. Discharge characteristics of the HAFC setup were estimated in a CV mode. An IPC-Pro potentiostat was used to record cyclic voltammograms at a potential scan rate of 10 mV s^{-1} in the range from the open circuit voltage (OCV) to 0.2 V. CVs were recorded after the MEA reached an operational mode, i.e., after prolonged cycling in the voltage range mentioned above.

Dependences of the current and power densities on the cell voltage measured at room temperature without excess hydrogen pressure and additional membrane humidification are shown in Fig. 8. As can be seen from the Figure, at the cell voltage 0.5 V the values of power density and current density for MEA with the PtFe/C cathode catalyst amounted to 135 mW cm^{-2} and 260 mA cm^{-2}, respectively, and those for MEA with conventional platinum catalyst were almost twice lower—73 mW cm^{-2} and 145 mA cm^{-2}, correspondingly. These results are in agreement with the data on the oxygen reduction at the synthesized catalysts obtained in TFRDE experiments.

Thus, at least some of the synthesized cluster-based catalysts seem promising candidates for application in low temperature HAFC. Nevertheless, the long-term MEA operation may result in the membrane poi-

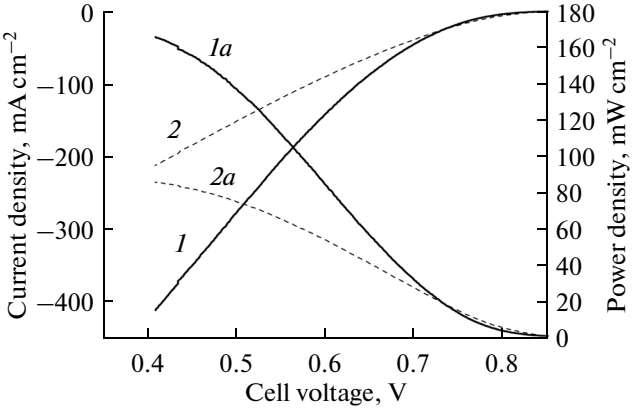

Fig. 8. Dependences of current density (*1*, *2*) and power density (*1a*, *2a*) on the unit fuel cell voltage for MEA with PtFe/C (*1*, *1a*) or commercial Pt/C (*2*, *2a*) cathode catalyst and Nafion 212 membrane measured at room temperature in a laboratory HAFC setup.

soning due to the non-noble components dissolution under polarization, and this problem is still to be studied.

Thus, the studies performed showed that the proposed method of catalyst synthesis using coordination compounds of Pt and other metals allows manufacturing of the oxygen electroreduction catalysts with a given composition, the specific characteristics of the obtained catalysts being not inferior to those of commercially available Pt-based catalysts. Power performance of MEA with the synthesized PtFe/C catalyst tested in a unit hydrogen-air fuel cell at room temperature was considerably better than that of MEA with a conventional platinum catalyst. At the same time, further optimization of the synthesis process appears essential in order to provide higher homogeneity of the catalyst particles by size and their more uniform distribution over the support surface. Besides, it is necessary to carry out a more detailed monitoring of the catalysts activity and their surface and bulk composition in the course of prolonged operation.

ACKNOWLEDGMENTS

This work was supported by the Federal Agency of the Scientific Organizations (FASO RF).

REFERENCES

1. Paffet, M.T., Beery, J.G., and Gottesfeld, S., *J. Electrochem. Soc.*, 1988, vol. 135, p. 1431.
2. Beard, B.C. and Ross, P.N., *J. Electrochem. Soc.,* 1990, vol. 137, p. 3368.
3. Neergat, N., Shukla, A., and Gandhi, K.S., *J. Appl. Electrochem.,* 2001, vol. 31, p. 373.
4. Toda, T., Igarashi, H., and Watanabe, M., *J. Electroanal. Chem.,* 1999, vol. 460, p. 258.
5. Jalan, V. and Taylor, E.J., *J. Electrochem. Soc.*, 1983, vol. 130, p. 2299.
6. Paulus, U.A., Wokaum, A., Scherer, G.G., et al., *Electrochim. Acta,* 2002, vol. 47, p. 3787.
7. Paulus, U.A., Wokaum, A., Scherer, G.G., et al., *J. Phys. Chem.*, *B*, 2002, vol. 106, p. 4181.
8. Murthi, V.S., Urian, R.C., and Mukerjee, S., *J. Phys. Chem., B*, 2004, vol. 108, p. 11011.
9. Yang, H., Alonso-Vante, N., Leger, J.-M., and Lamy, C., *J. Phys. Chem.*, *B*, 2004, vol. 108, no. 6, p. 1938.
10. Koffi, R.C., Coutanceau, C., Garnier, E., et al., *Electrochim. Acta,* 2005, vol. 50, p. 4117.
11. Tyumentsev, M.S., Zubavichus, Ya.V., Shiryaev A.A., and Anan'ev, A.V., *Radiochemistry,* 2014, vol. 56, no. 2, p. 150.
12. Tyumentsev, M.S., Anan'ev, A.V., and Shiryaev, A.A., *Dokl. Phys. Chem.,* 2013, vol. 450, p. 142.
13. Grinberg, V.A., Kulova, T.L., Maiorova, N.A., et al., *Russ. J. Electrochem.*, 2007, vol. 43, no. 1, p. 75.
14. Svergun, D.I., *J. Appl. Cryst.*, 1992, vol. 25, p. 495.
15. Delime, F., Leger, J.-M., and Lamy, C., *J. Appl. Electrochem.*, 1998, vol. 28, p. 27.
16. Maiorova, N.A., Mikhailova, A.A., Khazova, O.A., and Grinberg V.A., *Russ. J. Electrochem.*, 2006, vol. 42, no. 4, p. 331.
17. Mukerjee, S., Srinivasan, S., and Soriaga, M.P., *J. Electrochem. Soc.,* 1995, vol. 45, no. 5, p. 1409.
18. Paulus, U.A., Schmidt, T.J., Gasteiger, H.A., and Behm, R.J., *J. Electroanal. Chem.*, 2001, vol. 495, p. 134.